Could the two anticyclonic eddies during winter 2003/2004 be reproduced and predicted in the northern south China sea?

Dazhi Xu [1,3], Wei Zhuang[4], Youfang Yan [2*]

[1]South China Sea Marine Prediction Center, State Oceanic Administration, Guangzhou, China

[2]South China Sea Institute of Oceanology, Chinese Academic of Science, Guangzhou, China

[3]Nansen Environmental and Remote Sensing Center, Bergen, Norway

[4]State Key Laboratory of Marine Environmental Science & College of Ocean and Earth Sciences, Xiamen University, Xiamen 361102, China

Abstract

Great progress has been made in understanding the mesoscale eddies and their role on the large-scale structure and circulation of the oceans. However, many questions still remain to be resolved, especially with regard to the reproductivity and predictability of mesoscale eddies. In this study, the reproductivity and predictability of mesoscale eddies in the Northern SCS (NSCS), a region with strong eddy activity, are investigated with a focus on two typical anticyclonic eddies (AE1 and AE2) based on a HYCOM-EnOI Assimilated System. The comparisons of assimilated results and observations suggest that generation, evolution and propagation paths of AE1 and AE2 can be well reproduced and forecasted when the observed amplitude >8 cm (or the advective nonlinearity parameter U/c greater than 2), although their forcing mechanisms are quite different. However, when their amplitudes are less than 8 cm, the generation and decay of these two mesoscale eddies cannot be well reproduced and predicted by the system. This result suggests, in addition to dynamical mechanisms, the spatial resolution of assimilation observation data and numerical models must be taken into account in reproducing and predicting mesoscale eddies in the NSCS.

Keywords: HYCOM; EnOI; Northern South China Sea; Mesoscale eddy; Predictability

1. Introduction

Equivalent to the synoptic variability of the atmosphere, ocean mesoscale eddies are often described as the "weather" of the ocean, with typical spatial scales of ~100 km and time scales of a month (Wang et al., 1996; Liu et al., 2001; Chelton et al., 2011). The mesoscale eddy is characterized by temperature and salinity anomalies with associated flow anomalies, exhibiting different properties to their surroundings, thus allowing them to control the strength of mean currents and to transport heat, salt, and biogeochemical tracers around the ocean. The motion of mesoscale eddies would be a straight line, if eddies freely propagate in open ocean. However, most of eddies may have interaction with topography, strong currents (western boundary current), eddies during their lifetime. The motion of eddy will be modified and even split when approaching an island (Yang et al., 2017). It is also recognized that western boundary is graveyard of eddies (Zhai et al., 2010). The dynamical processes such as splitting and/or merging of eddies can also make termination and/or genesis of eddies in open ocean (Li et al., 2016). Thus, the dynamical processes make that the prediction of eddy motion is a challenge for ocean simulation. Although today, the beauty and complexity, the temporal and spatial variability, the eddy energy and tracking and the effects on atmosphere of these mesoscale features can be seen by viewing high resolution satellite images or numerical model simulations (Yang et al., 2000; Fu et al., 2010; Morrow and Le Traon, 2012; Frenger et al., 2013), the operational forecasts of the mesoscale eddy still pose a big challenge because of its complicated dynamical mechanisms and high nonlinearity (Woodham et al., 2015; Treguier et al., 2017; Vos et al., 2018). A recent

example is the explosion of the Deepwater Horizon drilling platform in the northern Gulf of Mexico in 2010 where an accurate prediction of the position and propagation of the Loop Current eddy was essential in determining if the spilled oil would be advected to the Atlantic Ocean or still remain within the Gulf (Treguier et al., 2017).

Similar to Gulf of Mexico, the South China Sea (SCS) is also a large semi-closed marginal sea, in the northwest Pacific, connecting to the western Pacific through the Luzon Strait (Fig. 1). Forced by seasonal monsoon winds, the intrusion of Kuroshio Current (KC), Rossby waves and the complex topography, SCS and especially the Northern SCS (NSCS) exhibits significant mesoscale eddy activity (Fig. 2). Many studies have tried to investigate mesoscale eddies in the NSCS (Wang et al., 2003; Jia et al., 2005; Wang et al., 2008). Based on the potential vorticity conservation equation and in-situ survey data, Yuan and Wang (1986) pointed out that the bottom topography forcing might be the primary factor for the formation of anticyclonic eddies northeast of Dongsha Islands (DIs). Using survey CTD data in September 1994, Li et al. (1998) recorded evidence of anticyclonic eddies in the NSCS and suggested these anticyclonic eddies are probably shed from the KC. Investigations by Wu et al. (2007) showed that westward propagating eddies in the NSCS originate near the Luzon Strait rather than coming from the western Pacific. Based on the altimeter, the trajectory of drift and the hydrological observations data, Wang et al. (2008) studied the evolution and migration of two anticyclonic eddies in the NSCS during winter of 2003/2004. As they described, the AE1 generated by interaction of the unstable rotating fluid with the sharp topography of DIs firstly appeared near DIs on the 10th of December 2003 (see Fig. 3).

74 Then it began to move southwestward with its amplitude decreasing gradually. During
75 the movement of AE1, another anticyclonic eddy (AE2) was shed and developed from
76 the loop current of Kuroshio near the Luzon Strait on the 14th of January 2004. The
77 amplitude of AE2 was then increased when it propagated southwestward (Fig. 3d-3f).
78 About five weeks later, AE2 reached its maximum in amplitude and then lasted around
79 three weeks in its mature state. During its decay phase, AE2 moved southwestward
80 quickly with its amplitude decreasing, and finally disappeared at the location of 114°E,
81 18°N on the 7th of April 2004. Meanwhile, AE1 continued moving to southwest and
82 eventually disappeared southeast of Hainan. In addition to physical characteristics, the
83 phytoplankton community at these two eddies have also been studied by Huang et al.
84 (2010). These studies improved our understanding of activities of mesoscale eddy and
85 its possible dynamical mechanisms in the NSCS.

86 Despite the activities and possible dynamical mechanisms of mesoscale eddies in the
87 NSCS having received much attention in past decades, studies on the reproductivity
88 and predictability of mesoscale eddies in the NSCS are still rare. As mentioned above,
89 mesoscale eddies are not only related to complicated dynamical mechanisms but also
90 involve strong nonlinear processes (Oey et al., 2005); they are not a deterministic
91 response to atmospheric forcing. The quality of mesoscale eddies forecasting will
92 depend primarily on the quality of the initial conditions. Ocean data assimilation, which
93 combines observations with the numerical model, can provide more realistic initial
94 conditions and thus is essential for the prediction of mesoscale eddies. As shown by
95 previous studies, after assimilating altimeter data into ocean models, the ocean currents

in the southern SCS (Xiao et al., 2006) and the realism of three largest eddies in the SCS during Typhoon Rammasun (Xie et al., 2018) have been improved. Furthermore, some studies show that the ocean model including tides or assimilated altimeter data with reasonable MDT, can provide more realistic initial conditions (Xie et al., 2011; Xu et al., 2012). The above studies show that the mesoscale eddies in the SCS are reproducible, but the predictability of mesoscale eddies is rare. In this study, we assessed the reproduction and predictability of two typical anticyclonic eddies (Wang et al., 2008), chosen as representing different generation mechanisms and surviving long enough to be useful, with focus on their generation, evolution and decay processes by a series of numerical experiments based on a Chinese Shelf/Coastal Seas Assimilation System (CSCASS; Li, 2009; Li et al., 2010; Zhu, 2011) along with the observation data from surface drifter trajectories and satellite remote sensing.

2. Datasets and Methodologies

2.1 Datasets

In this study, altimetric data in 2003-2004 was selected, including along-track SLA, totaling 29 passes (about 9300 points) over the domain of CSCS. Considering the noise of SLA measurement in the shallow seas, data for the shallow areas with depth<400 m was excluded. In order to verify, the merged SLA based on Jason-1, TOPEX/Poseidon, ERS-2 and ENVISAT (Ducet et al., 2000) provided by Archiving, Validation and Interpretation of Satellites Oceanographic data (AVISO) at Centre Localization Satellite (CLS, ftp://ftp.aviso.oceanobs.com/global/nrt/) with 1/4° x 1/4° resolution and weekly

117 average are used. In addition, because the SLA present only the anomalies relative to a
118 time-mean sea level field, a new mean dynamic topography (nMDT), which has been
119 corrected using iterative method by Xu et al. (2012), was used to calculate the realistic
120 sea level in this study.

121 In addition to SLA datasets, the daily OISST from the National Oceanic and
122 Atmospheric Administration's (NOAA) National Climatic Data Center
123 (ftp://eclipse.ncdc.noaa.gov/pub/OI-daily-v2/NetCDF/), which was merged by an
124 optimum interpolation method (Reynolds et al., 2007) based on the Infrared SST
125 collected by the Advanced Very High Resolution Radiometer sensors on the NOAA
126 Polar Orbiting Environmental Satellite and SST from Advanced Microwave Scanning
127 Radiometer for the Earth Observing System, are also used. The daily OISST's biases
128 were fixed using in situ data from ships and buoys. The dataset between 2003 and 2004
129 was used in this study, with a spatial resolution of 1/4°×1/4°. In addition, the surface
130 drifting buoy data from the World Ocean Circulation Experiment (WOCE,
131 ftp://ftp.aoml.noaa.gov/pub/phod/buoydata/) are also used. Three drifters were
132 designed to drift at the surface within the upper 15 m and tracked by the ARGOS
133 satellite system. Positions of the drifters were smoothed using a Gaussian-filter scale of
134 24 h to eliminate tidal and inertial currents, and were subsampled at 6 h intervals
135 (Hamilton et al., 1999).

136 **2.2 Method of identify the mesoscale eddies**

137 Similar to the standard of Cheng et al. (2005) and Chelton et al. (2011), we identify
138 the mesoscale eddies in this study as follows: 1) there must be a closed contour on the

merged SLA; 2) there must be one maximum or minimum inside the area of the closed contour for anticyclonic or cyclonic eddy; 3) the difference between the extremum and the outermost closed SLA contour, that is, the amplitude of the mesoscale eddy, must be greater than 2 cm; and 4) the spatial scale of the eddy should be 45-500 km. In addition, the amplitude (A) of an eddy is defined here to be the magnitude of the difference between the estimated basal height of the eddy boundary and the extremum value of SSH within the eddy interior: $A=|h_{ext}-h_0|$.

2.3 Ocean model

We here used a three-dimensional hybrid coordinate ocean model (HYCOM; Halliwell et al., 1998; 2000; Bleck, 2002; Halliwell, 2004; Chassignet et al., 2007) to provide a dynamical interpolator of observation data in the assimilation system. HYCOM is a primitive equation general ocean circulation model with vertical coordinates: isopycnic coordinate in the open stratified ocean, the geopotential (or z) coordinate in the weakly stratified upper ocean, and the terrain following sigma-coordinate in shallow coastal regions.

In this study, HYCOM was implemented in the Chinese shelf/coastal seas with a horizontal resolution of 1/12°×1/12°, and in the remaining regions with 1/8°×1/8°, the model domain is from 0°N to 53°N and from 99°E to 143°E, the detail model domain and grid can refer to the inset panel of Fig.1. The vertical water column from the sea surface to the bottom was divided into 22 levels. The K-Profile Parameterization (KPP; Large et al., 1994), which has proved to be an efficient mixing parameterization in many oceanic circulation models, was used here. The bathymetry data of the model domain

were taken from the 2-Minute Gridded Global Relief Data (ETOPO2).

To adjust the model dynamics and achieve a perpetually repeating seasonal cycle before applying the interannual atmospheric forcing, the model was initialized with climatological temperature and salinity from the World Ocean Atlas 2001 (WOA01; Boyer et al., 2005) and was driven by the Comprehensive Ocean-Atmosphere Data Set (COADS; Woodruff et al., 1987) in the spin-up stage. After integrating ten model years with climatological forcing, the model was forced by the European Center for Medium-Range Weather Forecasts (ECMWF) 6-hourly reanalysis dataset (Uppala et al., 2005) from 1997 to 2003. The wind velocity (10-m) components were converted to stresses using a stability dependent drag coefficient from Kara et al. (2002). Thermal forcing included air temperature, relative humidity and radiation (shortwave and longwave) fluxes. Precipitation was also used as a surface forcing from Legates and Willmott (1990). Surface latent and sensible heat fluxes were calculated using bulk formulae (Han, 1984). Monthly river runoff was parameterized as a surface precipitation flux in the ECS, the SCS and Luzon Strait (LS) from the river discharge stations of the Global Runoff Data Centre (GRDC) (http://www.bafg.de), and scaled as in Dai et al. (2002). Temperature, salinity and currents at the open boundaries were provided by an India-Pacific domain HYCOM simulation at 1/4°×1/4° spatial resolution (Yan et al., 2007). Surface temperature and salinity were relaxed to climatology on a time scale of 100 days. Both two-dimensional barotropic fields such as Sea Surface Height and barotropic velocities, and three-dimensional baroclinic fields such as currents, temperature, salinity and density were stored daily.

2.4 The assimilation scheme

The ensemble optimal interpolation scheme (EnOI; Oke et al., 2002), which is regarded as a simplified implementation of the Ensemble Kalman Filter (EnKF), aims at alleviating the computational burden of the EnKF by using stationary ensembles to propagate the observed information to the model space. The data assimilation schemes can be briefly written as (Oke et al., 2010):

$$\vec{\psi}^a = \vec{\psi}^b + K(\vec{d} - H\vec{\psi}^b) \tag{1}$$

$$K = P^b H^T [HP^b H^T + R]^{-1} \tag{2}$$

where $\vec{\psi}$ is the model state vectors including model temperature, layer thickness and velocity; Superscripts a and b denote analysis and background, respectively; $\vec{d}$ is the measurement vector that consists of SST and SLA observations; K is the gain matrix; and H is the measurement operator that transforms the model state to observation space. P is the background error covariance and R is the measurement error covariance. In EnOI, Eq. 2 can be expressed as:

$$K = \alpha(\sigma \circ P^b)H^T [\alpha H(\sigma \circ P^b)H^T + R]^{-1} \tag{3}$$

where α is a scalar that can tune the magnitude of the analysis increment; σ is a correlation function for localization; and P^b is the background error covariance which can be estimated by

$$P^b = A'A'^T/(n-1) \tag{4}$$

In Eq. 4, n is the ensemble size, A' is the anomaly of the ensemble matrix, $A = (\psi_1, \psi_2, \cdots, \psi_N) \in \Re^{n \times N}$ ($\psi_i \in \Re^N (i = 1, \cdots, n)$ is the ensemble members, N is the

dimension of the model state, representing usually the model variability at certain scales by using a long-term model run or spin-up run. More detailed description and evaluation of the CSCASS are in Li et al. (2010) and Xu et al. (2012).

3. Results

3.1 The reproduction of anticyclonic eddies AE1 and AE2 in the NSCS

In order to investigate whether the evolution and migration features of these two eddies can be reproduced by the CSCASS or not, we firstly set up an assimilation experiment named As_exp (see Fig. 4, black line) for AE1 and AE2. In this experiment, the observed SST and SLA are both assimilated into CSCASS every 3 days. To meet dynamic adjustment, the first assimilation was performed on the 27th of September 2003, two months prior to the generation of AE1.

Base on the As_exp experiment output, we use the observations SLA to evaluate the uncertainty of CSCASS in the research area. In this study, we calculated the weekly mean RMS error (RMSE) of the As_exp /control experiments output and observations for SLA. As the result indicates, the RMSE for the As_exp is between 6 cm to 14 cm, while RMSE for the control is between 10 cm to 18 cm. This result suggested that data assimilation improved effectively the SLA field and had a beneficial impact on model results in this area.

In addition, we also use the Advective Nonlinearity Parameter U/c (ANP, Chelton et al., 2011; Li et al., 2014; 2015; 2016; Wang et al., 2015) as a criterion to estimate the eddy forecast ability of the CSCASS. As fig. 5 shows, when the ANP is greater than 2 (that is the amplitude greater than 8 cm in our runs) AE2 can be reproduced by the

CSCASS.

Besides, we also use the independent evaluation, Fig.6 compares the assimilating results of AE1 with observations both from the satellite remote sensing and drifter buoys trajectories of number 22517, 22918 and 22610 between December 3rd 2003 and February 18th 2004. From Fig. 6 and Table 1, we can see that the generation and movement of AE1 can be well reproduced by the CSCASS; the pink curves (assimilation) match well with those of black (satellite observations) and dotted lines (the trajectories of drifter buoys). In addition, the spatial pattern of AE1 can also be well revealed by the CSCASS: the meridional and zonal radii of AE1 detected by the assimilation are 163 km and 93 km, which are almost equal to that of observations (148 km and 79 km). The migration path of AE1 can also be well reproduced by the CSCASS (see Fig. 6, black and pink line) until its amplitude decays to less than 8 cm. In addition to AE1, the generation and evolution of AE2 are also evaluated. As shown Fig. 7, the evolution and propagation pathway of AE2 (Fig. 7b-7j), e.g. moving northwestward firstly and then southwestward, can generally be reproduced by the CSCASS, although its initial location shows a slight southward bias in the simulation (Fig. 7a). Similar to the results of AE1, discrepancies between model and observations become larger again during the decay phase of AE2.

In general, the comparison of assimilation SLA with that of satellite observation and the trajectories of drifter buoys suggested that the generation, development and the propagation of AE1 and AE2 can be reproduced by the CSCASS when their observed amplitude is greater than 8 cm (or the ANP greater than 2). However, when their

amplitudes are relatively small, less than 8 cm, the features of these two mesoscale eddies are not well reproduced by the CSCASS. This may be related to the value setting of parameter α, the localization length scale, and insufficient spatial resolution of assimilated SSH or the numerical model (Counillon and Bertino, 2009).

3.2 The predictability of these anticyclonic eddies in the NSCS

Since the generation, development and the propagation of AE1 and AE2 can be well reproduced by the CSCASS when their amplitude >8 cm (or the ANP greater than 2), as mentioned above, in this section we further use the CSCASS to investigate the predictability of these two eddies. According to the generation, evolution and migration of these two eddies, we designed six forecast experiments, hereafter referred to as Exp1 to Exp6 (see Fig.4) to investigate their predictability. The model's initial state prior to each of the six forecast experiments is constrained by assimilating satellite SLA and SST before. Based on the initial state, each experiment is run forward 30 days with the forcing of 6-hourly wind, surface heat flux, and monthly mean river runoff, etc. The first experiment, named Exp1, is applied on the 29th of November 2003, which tends to study whether the generation of AE1 can be forecasted or not. Exp2 is implemented on the 10th of December 2003 and is used to study whether the development and the migration of AE1 can be forecasted. Exp3 is run based on the initial state on the 31th of December 2003 and used to show whether the generation of AE2 and the continued migration of AE1 can be forecasted. In order to investigate whether the continued evolution of AE1 and AE2 can be forecasted, Exp4 is applied on the 21th of January 2004. Exp5 is set up to reveal whether the attenuation of AE1 and the evolution of AE2

can be forecasted, while Exp6 which is applied on the 29th of February 2004 was designed to find out whether the disappearance of AE1 and AE2 can be forecasted.

The prediction results of Exp1 are shown in Fig. 8. In Fig. 8a, we can see that the forecast is almost coincident with the satellite observation and the trajectory of drift buoys, indicating that the generated position of AE1 can be well forecasted by the CSCASS. In addition, the initial migration of AE1 can also be forecasted by the CSCASS (see Fig. 8a and 8f). In order to evaluate the forecasted amplitude of AE1, the amplitude and the distance of eddy centers between the observation and the forecast are also quantified (Table 2: EXP1). From Table 2: EXP1, we can see that the amplitude of forecasting matches well with that of observation, although its amplitude is slightly larger than that of observation. After 4 weeks, the amplitude of the forecast is still close to those of the observation, suggesting that the generation of AE1 can be well predicted by the CSCASS.

In order to find out whether the development and movement path of AE1 can be predicted after generation, we continue to carry out Exp2. As shown by the observation (Fig. 9), AE1 moves southwestward along the continental shelf with its amplitude decreasing and again increasing after its generation. This observed southwestward movement is also predicted by the CSCASS (see pink closure curve in Fig. 9a-9d), although a sudden southwestward movement cannot be well predicted (Fig. 9f). In addition, the first attenuation and then enhancement of AE1 was also predicted by the CSCASS (see Table 2 and Fig. 9b). On the whole, the development and movement path of AE1 can be well predicted by CSCASS for the first four weeks after its generation.

After that, the errors between observation and prediction increase significantly, and by the fifth week, the distance between the center of the prediction and the observation become larger, more than 100 km (see Fig. 9e).

For further analysis, we carry out Exp3, to look at whether the continued evolution of AE1 and the generation of AE2 can be predicted. This experiment is carried out based on the initial condition of the assimilation on the 31st of December 2003 and the corresponding results are shown in Fig. 10 and Table 2. As shown by the prediction (Fig. 10, Table 2), although with a slightly weak amplitude, the CSCASS can reproduce AE1 after assimilating SLA and SST and predicted its development trend. In addition, the movement path of AE1 cannot be accurately predicted at this period, for instance, the observed AE1 moves directly to southwest (see red solid line and solid circle in Fig. 10f), but the predicted movement is firstly toward northeast, then turns to southwest (see blue solid line and solid circle in Fig. 10f). The generation of AE2 cannot be predicted in Exp3, which may be related to the smaller amplitude (<8 cm) of AE2 at this period.

The purpose of Exp4 is to look at whether the evolution of AE1 and AE2 can both be reasonably predicted. Since this experiment mainly focuses on the evolution of AE1 and AE2, Fig. 11 shows only the evolution of AE2 from the second week after generation, that is, from the beginning on the 21st of January 2004 to the fifth week. As shown in Fig. 11, Table 2 and Fig. 14d, the trends of amplitude variation of both eddies can be well predicted with the decreasing of AE1 and slow increasing of AE2. For AE1, the results of the prediction and observation are very close in the first two weeks, with

the centres of the two almost coinciding. The central position of the prediction and observation began to deviate after the third week. For AE2, although the amplitude and movement path are not predicted well at its initial stage, the prediction is slowly approaching to the observation during third to fifth week, and distance between the center of the prediction and the observation is reduced from 132 km at the beginning to 81 km at the end (see Fig. 14d the black solid line).

As mentioned above, the purpose of Exp5 is to investigate whether the decay of AE1 and the continued development of AE2 can be predicted. From Fig. 12, Table 2 and Fig. 14e, we can find that the CSCASS cannot predict the movement path of AE1 well in its decay stage: the distance between the center of the prediction and that of the observation is greater than 188 km, and movement direction of the two is not consistent (see red lines and dots in Fig. 12f). But the evolution and movement direction of AE2 can be well predicted at this stage. The amplitude of observation and prediction of AE2 are getting closer with time (Fig. 14e), although the speed of movement of AE2 given by prediction is slower than that of observation (see blue dashed lines and hollow dots in Fig. 12f).

The aim of Exp6 is to find whether the disappearance of AE1 and AE2 can be both predicted. As described in Fig. 13, the disappearance of AE1 cannot be well predicted owing to the low amplitude (less than 8 cm) of AE1 at this stage. Similarly, the disappearance of AE2 is also less accurately predicted by the CSCASS (Fig. 14f). The observed amplitude of AE2 decays continually at this stage, but the predicted amplitude is almost constant. In addition, there is large deviation of the direction of movement

between prediction and observation for AE2 (see the red solid line and dot in Fig. 13f).

4. Conclusions and challenges for forecasting of mesoscale eddy

In this paper, we carry out a series of assimilation and prediction experiments by the CSCASS to assess the production and predictability of mesoscale eddies in the NSCS, along with observations of satellite observed SST, SLA and the trajectory data of drift. The comparisons of AE1 and AE2 observations with CSCASS prediction experiments, which assimilate SLA and SST, show that when the amplitudes of mesoscale eddy are higher than 8 cm, the generation, development, decay and movement of eddies can be well reproduced, but when the amplitude of the mesoscale eddy is lower than 8 cm, the generation and disappearance of mesoscale eddy cannot be well reproduced.

The comparisons of AE1 and AE2 through six prediction experiments with observations also show that the generation, evolution and movement path of these two eddies with high amplitude (>8 cm or the ANP greater than 2) can be well predicted by the CSCASS, although the generation mechanism of these two eddies is quite different (Wang et al., 2008). However, when the amplitude of eddies becomes less than 8 cm, the generation position and the movement path cannot be well predicted by the CSCASS.

Our results suggested that for powerful mesoscale eddies, a good initial condition after assimilating observations can help to improve their reproduction and predictability. As mentioned above, the mesoscale eddies are related to strong nonlinear processes and are not a deterministic response to atmospheric forcing, thus the quality of mesoscale eddies forecast will depend primarily on the quality of the initial conditions. In addition,

the ability of the ocean numerical model to faithfully represent the ocean physics and dynamics is also crucial. Although data assimilation, which combines observations with the numerical model, can provide good initial conditions, it cannot make up for limitations of numerical model algorithms and in its resolution. Hence for high-resolution operational oceanography, numerical models need to be improved using more accurate numerical algorithms and resolution especially in the weakly stratified regions or on the continental shelf.

Furthermore, so far most of the information about the ocean variability is obtained remotely from satellites (SSH and SST), the information about the subsurface variability are very rare. Although a substantial source of subsurface data is provided by the vertical profiles (i.e., expendable bathy thermographs, conductivity temperature depth, and Argo floats), the datasets are still not sufficient to determine the state of the ocean. In addition, in order to accurately assimilate the SSH anomalies from satellite altimeter data into the numerical model, it is necessary to know the oceanic mean SSH over the time period of the altimeter observations (Xu et al., 2011; Rio et al., 2014). This is also a big challenge because the earth's geoid is not presented with sufficient spatial resolution when assimilating SSH in an eddy-resolving model. With the advent of the SWOT (Surface Water and Ocean Topography) satellite mission in 2020, it should be possible to better resolve and forecast the mesoscale features in eddy resolving ocean forecasting systems.

Acknowledgements:

This study is supported by the Marine Science and Technology Foundation of South China Sea Branch, State Oceanic Administration (grant 1447), the National Key Research and Development Program of China (2016YFC1401407), the Project of Global Change and Air-Sea interaction under contract No. GASI-03-IPOVAI-04, the National Natural Science Foundation of China (Grant No. 41731173, 41776037 and 41276027), and the China Scholarship Council (award to Xu Dazhi for 1 year's study abroad at Nansen Environmental and Remote Sensing Center).

References:

Bleck, R.: An oceanic general circulation model framed in hybrid isopycnic cartesian coordinates, Ocean Model., 4, 55-88, 2002.

Boyer, T. P., Levitus, S., Antonov, J. I., et al.: Linear trends in salinity for the World Ocean, 1955-1998, Geophy. Res. Lett., 32, 67-106, 2005.

Chassignet, E. P., Hurlburt, H. E., Smedstad, O. M., et al.: The HYCOM (Hybrid Coordinate Ocean Model) data assimilative system, J. Mar. Sys., 65, 60-83, 2007.

Chelton, D. B., Schlax, M. G., and Samelson, R. M.: Global observations of nonlinear mesoscale eddies, Progr. in Oceanogr., 91, 167-216, 2011.

Cheng, X. H., Qi, Y. Q., and Wang, W. Q.: Seasonal and Interannual Variabilities of Mesoscale Eddies in South China Sea, J. Trop. Oceanogr., 24, 51-59, 2005.

Counillon, F., and Bertino, L.: Ensemble Optimal Interpolation: multivariate properties in the Gulf of Mexico, Tellus, 61A, 296-308, 2009.

Dai, A., and Trenberth, K. E.: Estimates of freshwater discharge from continents: latitudinal and seasonal variations, J. Hydrometeor., 3, 660-685, 2002.

Ducet, N., LeTraon, P. Y., and Reverdin, G.: Global high-resolution mapping of ocean circulation from TOPEX/Poseidon and ERS-1 and-2, J. Geophy. Res., 105, 19477-19498, 2000.

Frenger, I., Gruber, N., Knutti, R., and Münnich, M.: Imprint of Southern Ocean eddies on winds, clouds and rainfall, Nat. Geosci., 6, 608-612, 2013.

Fu, L.-L., Chelton, D. B., Traon, P.-Y. L., et al.: Eddy dynamics from satellite altimetry, Oceanogr., 23, 14-25, 2010.

Halliwell, J. G. R.: Evaluation of vertical coordinate and vertical mixing algorithms in the HYbrid-Coordinate Ocean Model (HYCOM), Ocean Model., 7, 285-322, 2004.

Halliwell, J. G. R., Bleck, R., and Chassignet, E. P.: Atlantic Ocean simulations performed using a new Hybrid Coordinate Ocean Model (HYCOM), EOS, Fall AGU Meeting, 1998.

Halliwell, J. G. R., Bleck, R., Chassignet, E. P., et al.: Mixed layer model validation in Atlantic Ocean simulations using the Hybrid Coordinate Ocean Model (HYCOM), EOS, 80, OS304, 2000.

415 Hamilton, P., Fargion, G. S., and Biggs, D. C.: Loop Current eddy paths in the western Gulf of
416 Mexico, J. Phys. Oceanogr., 29, 1180-1207, 1999.
417 Han, Y.–J.: A numerical world ocean general circulation model: Part II. A baroclinic experiment,
418 Dyn. Atmos. Oceans, 8,141-172, 1984.
419 Huang, B. Q., Hua, J., Xu, H. Z., et al.: Phytoplankton community at warm eddies in the
420 northern South China Sea in winter 2003/2004, Deep Sea Res. Part II, 57, 1792-1798,
421 2010.
422 Jia, Y., Liu, Q., and Liu, W.: Primary studies of the mechanism of eddy shedding from the
423 Kuroshio bend in Luzon Strait, J. Oceanogr., 61, 1017-1027, 2005.
424 Kara, A. B., Rochford, P. A., and Hurlburt H E.: Air-sea flux estimates and the 1997-1998
425 ENSO event, Boundary-Layer Meteorol., 103, 439-458, 2002.
426 Large, W. G., McWilliams, J. C., and Doney, S. C.: Oceanic vertical mixing: a review and a
427 model with a nonlocal boundary layer parameterization, Rev. Geophys., 32, 363-403,
428 1994.
429 Legates, D. R., and Willmott, C. J.: Mean seasonal and spatial variability in gauge-corrected,
430 global precipitation, Int. J. Climatol., 10, 111-127, 1990.
431 Li, L., Nowlin, W. D., and Su, J, L.: Anticyclonic rings from the Kuroshio in the South China
432 Sea, Deep-Sea Res., Part I, 45, 1469-1482, 1998.
433 Li, Q. Y., and Sun, L.: Technical Note: Watershed strategy for oceanic mesoscale eddy splitting,
434 Ocean Sci., 11, 269-273, doi:10.5194/os-11-269-2015, 2015.
435 Li, Q. Y., Sun, L., and Lin, S.-F.: GEM: a dynamic tracking model for mesoscale eddies in the
436 ocean, Ocean Sci., 12, 1249-1267, doi:10.5194/os-12-1249-2016, 2016.
437 Li, Q. Y., Sun, L., Liu, S.-S., et al.: A new mononuclear eddy identification method with simple
438 splitting strategies, Remote Sens. Lett., 5, 65-72. Doi:10.1080/2150704X.2013.872814,
439 2014.
440 Li, X. C.: Applying a new localization optimal interpolation assimilation module to assimilate
441 sea surface temperature and sea level anomaly into the Chinese Shelf/Coastal Seas model
442 and carry out hindcasted experiment, Graduate University of the Chinese Academy of
443 Sciences, China, 92 pp, 2009.
444 Li, X. C., Zhu, J., Xiao, Y. G., et al.: A Model-Based Observation Thinning Scheme for the

445 Assimilation of High-Resolution SST in the Shelf and Coastal Seas around China, J.
446 Atmos. Oceanic Technol., 27, 1044-1058, 2010.
447 Liu, Z., Yang, H. J., and Liu, Q.: Regional dynamics of seasonal variability of sea surface height
448 in the South China Sea, J. Phys. Oceanogr., 31, 272-284, 2001.
449 Morrow, R., and Traon, P.-Y. L.: Recent advances in observing mesoscale ocean dynamics with
450 satellite altimetry, Adv. Spa. Res., 50, 1062-1076, 2012.
451 Oey, L. T., Ezer, T., and Lee, H. C.: Loop Current, rings and related circulation in the Gulf of
452 Mexico: a review of numerical models. In: Circulation in the Gulf of Mexico:
453 Observations and Models Volume 161, American Geophysical Union, 31-56, 2005.
454 Oke, P. R., Allen, J. S., Miller, R. N., et al.: Assimilation of surface velocity data into a primitive
455 equation coastal ocean model, J. Geophy. Res. Oceans, 107, 5-1-5-25, 2002.
456 Oke, P. R., Brassington, G. B., Griffin, D. A., et al.: Ocean data assimilation: a case for ensemble
457 optimal interpolation, Australian Meteorological and Oceanographic Journal, 59, 67-76,
458 2010.
459 Reynolds, R. W., Smith, T. M., Liu, C., et al.: Daily High-Resolution Blended Analyses for Sea
460 Surface Temperature, J. Climate, 20, 5473-5496, 2007.
461 Rio, M. H., Mulet, S., and Picot, N.: Beyond GOCE for the ocean circulation estimate:
462 Synergetic use of altimetry, gravimetry, and in situ data provides new insight into
463 geostrophic and Ekman currents, Geophy. Res. Lett., 41, 8918-8925, 2014.
464 Treguier, A. M., Chassignet, E. P., Boyer, A. L., et al.: Modeling and forecasting the "weather
465 of the ocean" at the mesoscale, J. Mar. Res., 75, 301-329, 2017.
466 Uppala, S., Kallberg, P., Simmons, A. J., et al.: The EAR-40 re-analysis, Q. J. R. Meteorol. Soc.,
467 131, 2961-3012, 2005.
468 Vos, M. D., Backeberg, B., and Counillon, F.: Using an eddy-tracking algorithm to understand
469 the impact of assimilating altimetry data on the eddy characteristics of the Agulhas system,
470 Ocean Dyn., 1-21, 2018.
471 Wang, D. X., Zhou, F. Z., and Qin Z. H.: Numerical simulation of the upper ocean circulation
472 with two-layer model, Acta Oceanol. Sin., 18, 30-40, 1996.
473 Wang, D., Xu, H., Lin, J., et al.: Anticyclonic eddies in the northeastern South China Sea during
474 winter 2003/2004, J, Oceanogr., 64, 925-935, doi: 910.1007/s10872-10008-10076-10873,

2008.

Wang, G., Su, J., and Chu, P. C.: Mesoscale eddies in the South China Sea observed with altimeter data, Geophy. Res. Lett., 30, 2121, doi: 10.1029/2003GL018532, 2003.

Wang, Z., Li, Q., Sun, L., Li, S., et al.: The most typical shape of oceanic mesoscale eddies from global satellite sea level observations, Front. Earth Sci., 9, 202-208. DOI 10.1007/s11707-014-0478-z, 2015.

Woodham, R. H., Alves, O., Brassington, G. B., et al.: Evaluation of ocean forecast performance for Royal Australian Navy exercise areas in the Tasman Sea, J. Oper. Oceanogr., 8, 147-161, 2015.

Woodruff, S. D., Slutz, R. J., Jenne, R. L., et al.: A comprehensive ocean-atmosphere data set, Bull. Am. Meteorol. Soc., 68, 1239-1250, 1987.

Wu, C. R., and Chiang, T. L.: Mesoscale eddies in the northern South China Sea, Deep-Sea Res., Part II, 54, 1575-1588, 2007.

Xiao, X. J., Wang, D. X., and Xu, J.-J.: The assimilation experiment in the southwestern South China Sea in summer 2000, Chin. Sci. Bull., 51, 31-37, 2006.

Xie, J. P., Bertino, L., Cardellach, E., et al.: An OSSE evaluation of the GNSS-R altimetery data for the GEROS-ISS mission as a complement to the existing observational networks, Remote Sens. Environ., 209, 152-165, 2018.

Xie, J. P., Counillon, F., Zhu, J., et al.: An eddy resolving tidal-driven model of the South China Sea assimilating along-track SLA data using the EnOI, Ocean Sci., 8, 609-627, 2011.

Xu, D. Z., Li, X. C., Zhu, J., et al.: Evaluation of an ocean data assimilation system in the marginal seas around China, with a focus on the South China Sea, Chin. J. Oceanol. Limnol., 29, 414-426, 2011.

Xu, D. Z., Zhu, J., Qi, Y. Q., et al.: Impact of mean dynamic topography on SLA assimilation in an eddy-resolving model, Acta Oceanol. Sin., 31, 11-25, 2012.

Yan, C. X., Zhu, J., and Zhou, G. Q.: Impacts of XBT, TAO, altimetry and ARGO observations on the tropic Pacific Ocean data assimilation, Adv. Atmos. Sci., 24, 383-398, 2007.

Yang, K., Shi, P., Wang, D. X., et al.: Numerical study about the mesoscale multi-eddy system in the northern South China Sea in winter, Acta Oceanol. Sin., 22, 27-34, 2000.

Yang, S., Xing, J., Chen, D., et al.: A modelling study of eddy-splitting by an island/seamount,

505 Ocean Sci., 13, 837-849, https://doi.org/10.5194/os-13-837-2017, 2017.
506 Zhai, X., Johnson, H. L., Marshall, D. P.: Significant sink of ocean-eddy energy near western
507 boundaries. Nat. Geosci., 3, 608-612, 2010.
508 Zhu, J.: Overview of Regional and Coastal Systems, Chapter 17 in Operational Oceanography
509 in the 21st Century. Edited by A. Schiller and G. B. Brassington, PP. 727, Springer Science,
510 Business Media B.V, 2011.
511 Zhuang, W., Du, Y., Wang, D. X., et al.: Pathways of mesoscale variability in the South China
512 Sea, Chin. J. Oceanol. Limnol., 28, 1055-1067, 2010.

Figures:

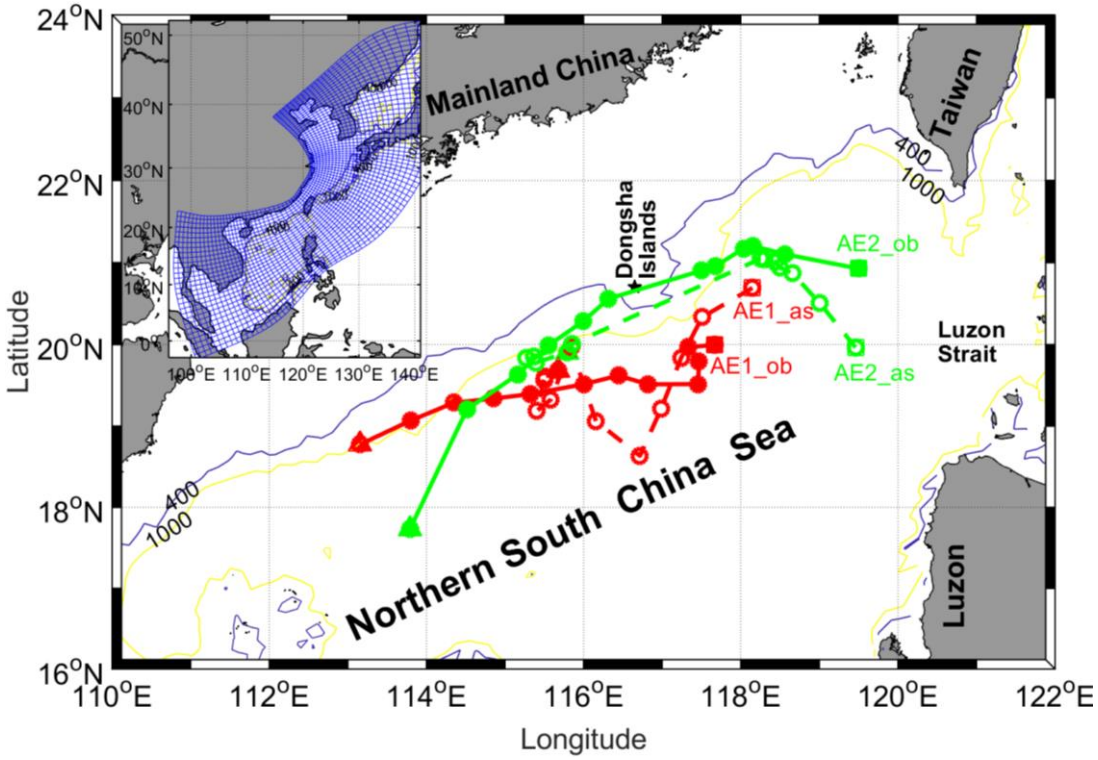

Fig. 1 Bathymetry of the northern South China Sea. The blue and yellow contour lines are the isolines of 400 m and 1000 m. The solid black Pentagram indicated Dongsha Islands. The migration path of AE1 and AE2 in the NSCS during December 2003~April 2004. Red solid (hollow) circle dots and solid (dash) lines indicated weekly passing position and migration path of observation (assimilation) AE1. Green solid (hollow) circle dots and solid (dash) lines indicated weekly passing position and migration path of observation (assimilation) AE2. The quadrangle and triangle denoted start and end position, respectively. The model domain of CSCSS (the inset panel), the curvilinear orthogonal model grid with 1/8-1/12° horizontal resolution (147×430) is denoted by the blue grid (at intervals of 10 grid cells here).

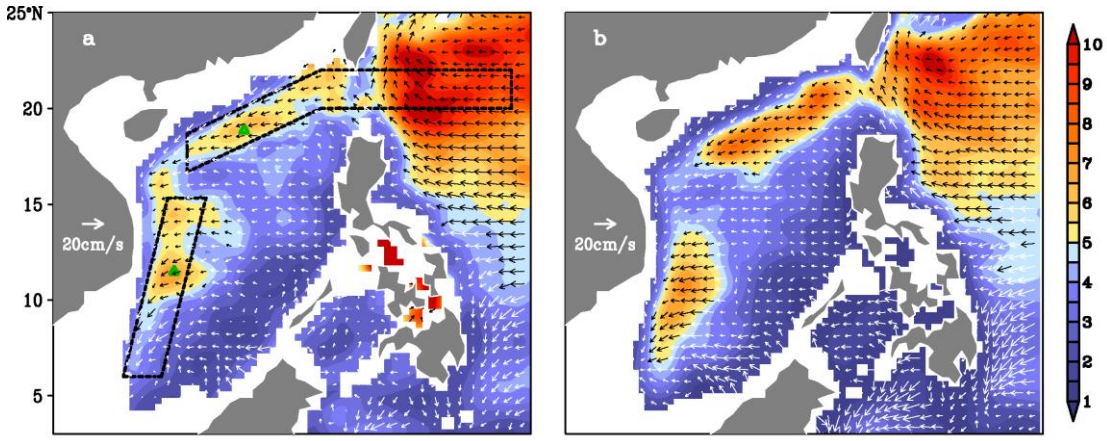

Fig. 2 Annual mean standard deviation of sea level mesoscale signals (color shading, unit: cm) and propagation velocities of the signals (vectors) derived from (a) altimeter observations; (b) OFES simulations. From Zhuang et al. (2010).

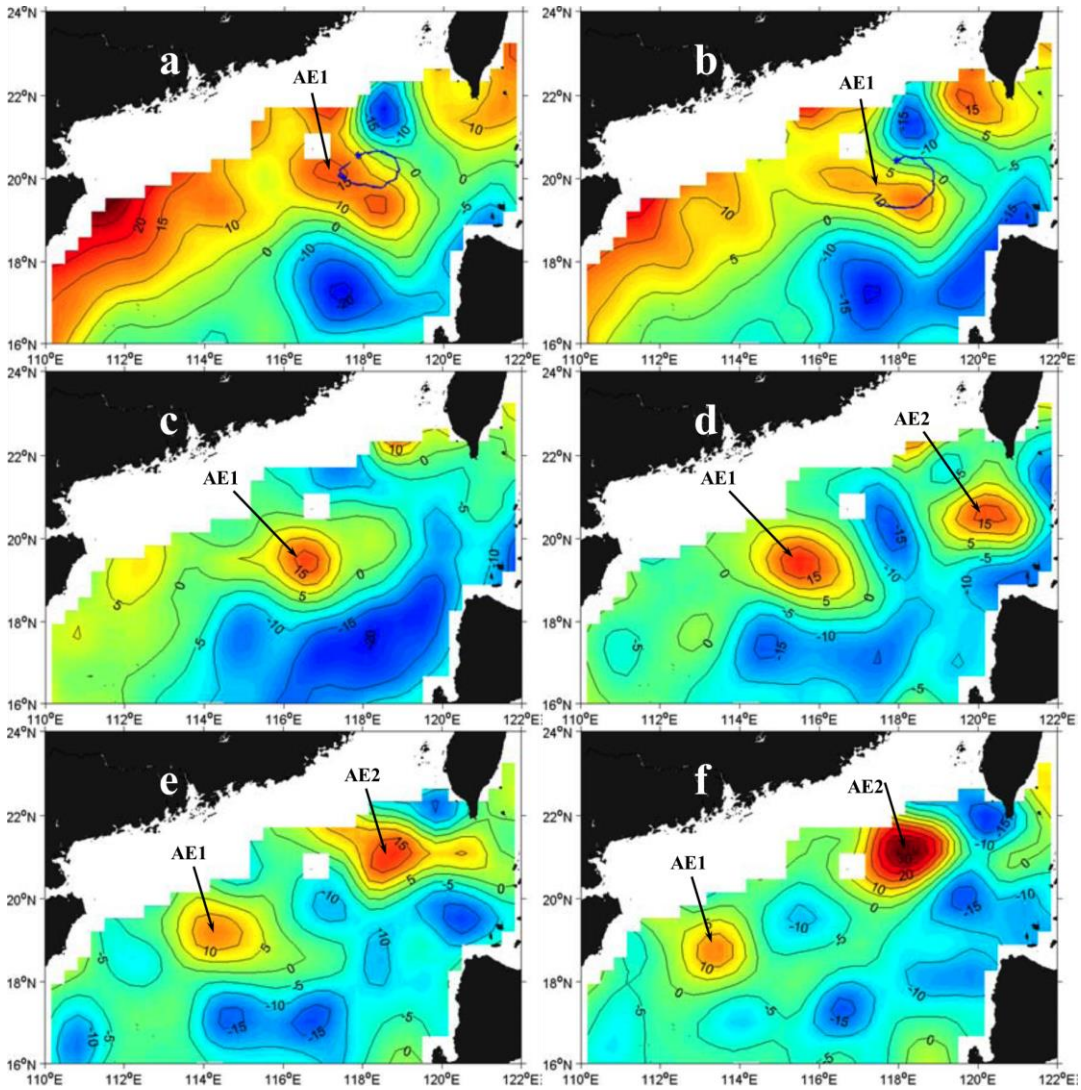

Fig. 3 Snapshots of SLA from satellite remote sensing datasets. Buoy 22918 trajectory (blue lines,

blue asterisk represents the initial position of buoy, as in Fig. 4) (a) from December 4-15, 2003 superposed on SLA field on December 10, 2003; (b) from December 16-23, 2003 superposed on SLA field on December 17, 2003; SLA field on (c) January 7, 2004; (d) January 21, 2004; (e) February 4, 2004; (f) February 18, 2004. From Wang et al. (2008).

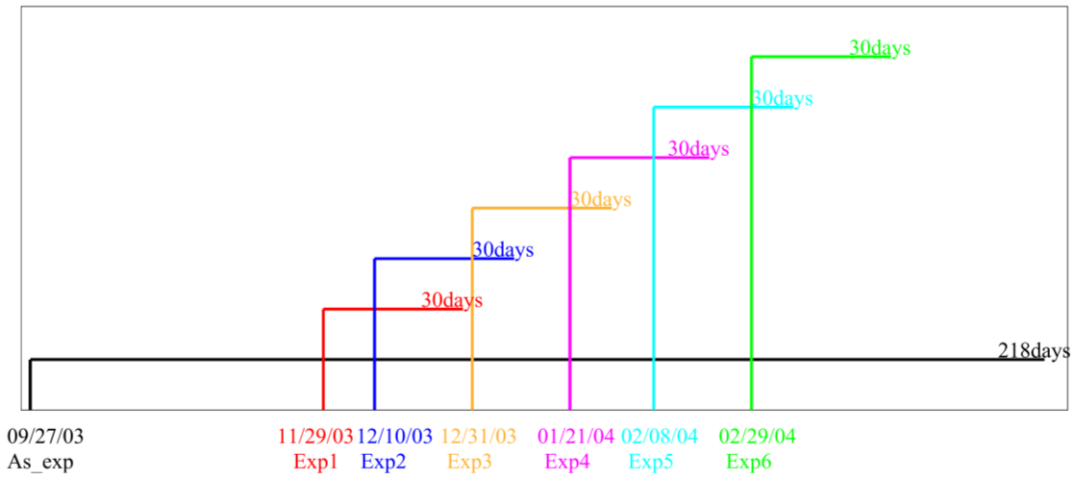

Fig. 4 The settings of assimilation and six forecast experiments, including the start and end date.

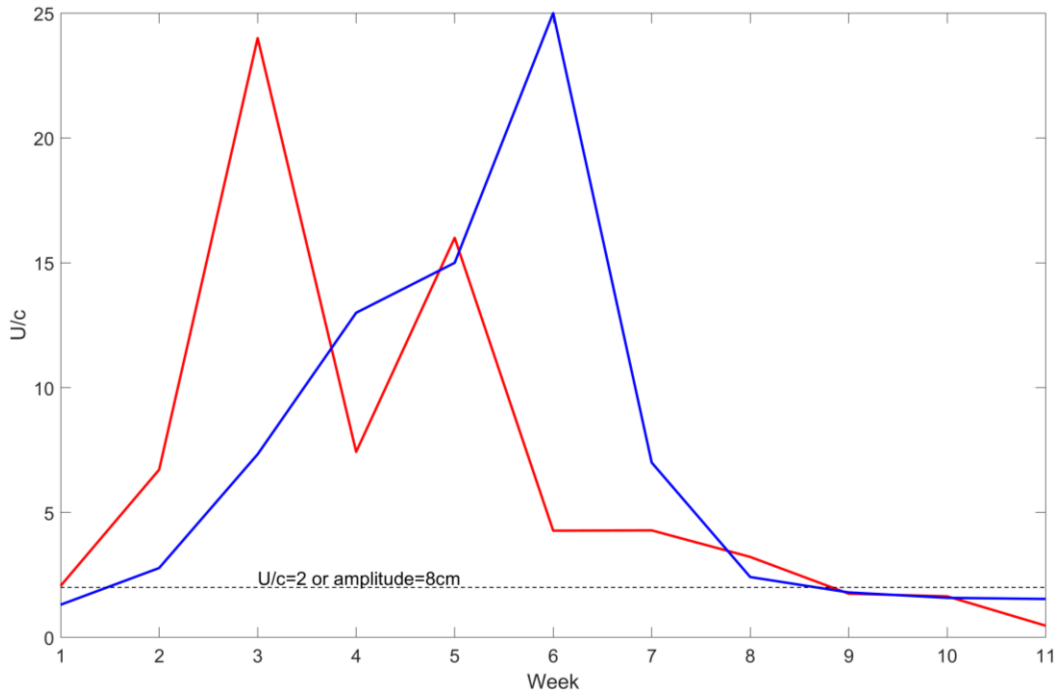

Fig. 5 The advective nonlinearity parameter U/c (ANP). The thick red (blue) curve indicates the ANP of the observations (As_exp experiment) of AE2, the dash line indicates the value of eddy amplitude at 8 cm or the ANP greater than 2.

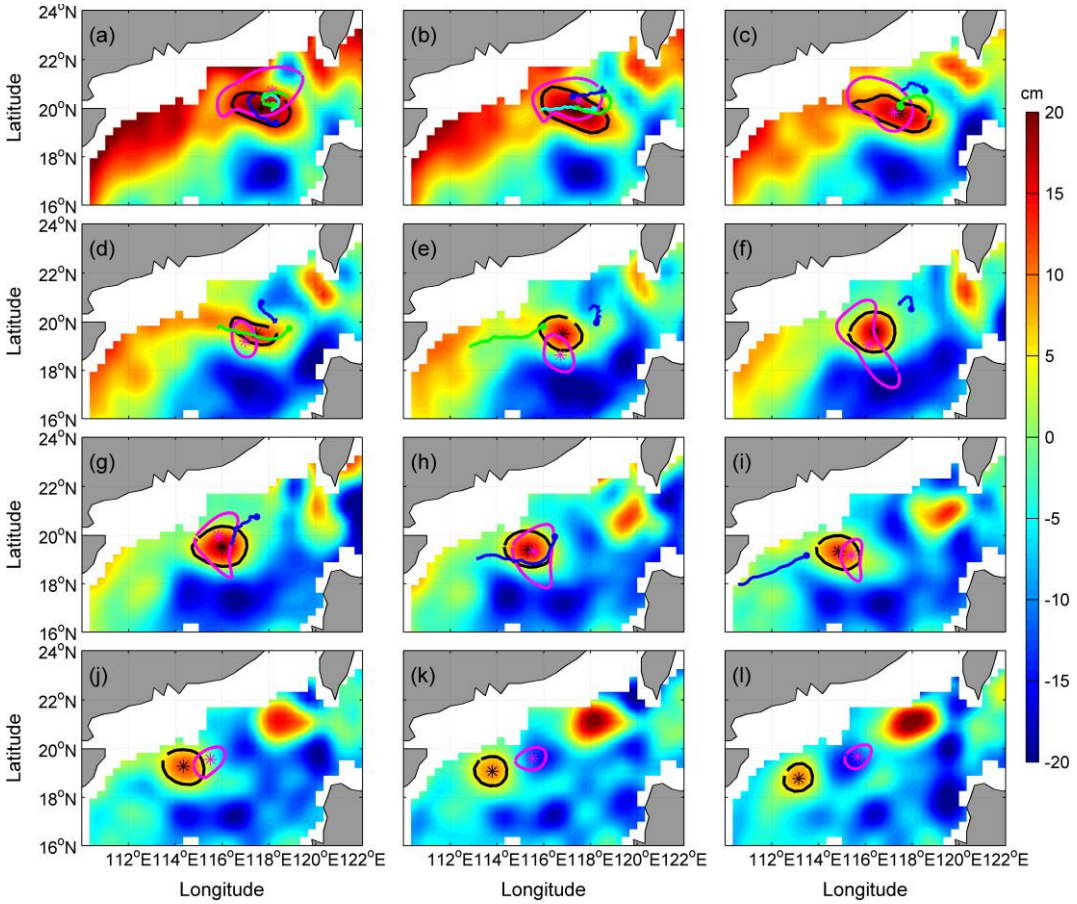

Fig. 6 Comparisons AE1 derived from weekly SLA of assimilation results and observation from satellite remote sensing during the period of December 2003~February 2004. Background color is SLA, "*" mark and closed lines indicated the center position and the outermost closed isoline of AE1, respectively, the black is from satellite observation SLA, the pink is from assimilation SLA. The cyan, green and blue solid circle lines indicated the start positions and trajectories of number 22517, 22918 and 22610 drifter buoys, respectively. (a)-(l) is SLA on the 3rd of December 2003~ the 18th of February 2004, respectively. Unit: cm.

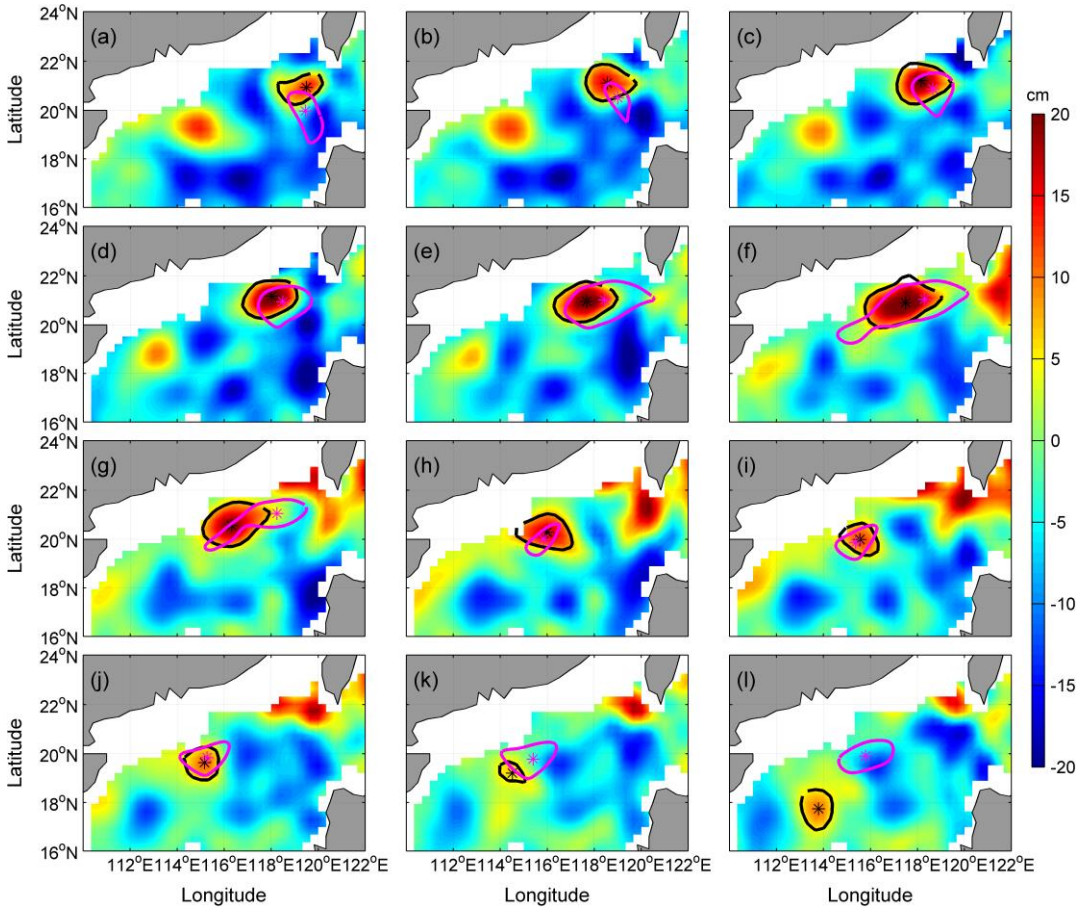

Fig. 7 The same as figure 6, But for AE2, the corresponding period is January 28th, 2003~April 14th, 20.

552

553 **Tables：**

554 Table 1 The amplitude of AE1 and AE2 derived from observation SLA and the assimilation SLA, and distance of eddy centers between the observation SLA's and
555 assimilation SLA's.

Weekly			1(2003/12/3)	2	3	4	5	6	7	8	9	10	11	12
AE1	Distance (km)		94	45	26	62	98	70	54	30	63	131	199	298
	Amplitude(cm)	Observed	8	10	9	8	8	13	13	11	8	8	4	6
		Assimilated	18	12	11	6	5	4	5	6	2	3	3	2
Weekly			1(2004/1/28)	2	3	4	5	6	7	8	9	10	11	12
AE2	Distance (km)		107	83	67	57	85	91	221	36	26	26	117	328
	Amplitude(cm)	Observed	7	12	18	17	17	16	15	10	7	6	N/A	6
		Assimilated	3	2	5	6	10	8	4	8	9	4	5	6

556

Table 2 The amplitude of AE1 and AE2 derived from observation SLA and the six forecast SLA, and distance of eddy centers between the observation SLA's and forecast SLA's.

Weekly				1	2	3	4	5
Exp1	Distance (km)			80	58	32	68	47
	Amplitude (cm)		Observed	8	10	9	8	8
			Forecasted	14	12	14	11	12
Exp2	Distance (km)			57	22	63	51	113
	Amplitude (cm)		Observed	10	9	8	8	13
			Forecasted	12	11	6	8	10
Exp3	Distance (km)			134	85	111	130	124
	Amplitude (cm)		Observed	13	13	11	8	8
			Forecasted	2	3	3	3	N/A
Exp4	AE1	Distance (km)		32	58	111	161	231
		Amplitude (cm)	Observed	11	8	8	4	6
			Forecasted	4	2	2	2	N/A
	AE2	Distance (km)		N/A	N/A	132	95	81
		Amplitude (cm)	Observed	N/A	N/A	12	18	17
			Forecasted	N/A	N/A	N/A	6	9
Exp5	AE1	Distance (km)		188	274	287	405	503
		Amplitude (cm)	Observed	4	6	2	N/A	N/A
			Forecasted	2	2	2	2	2
	AE2	Distance (km)		69	77	102	95	226
		Amplitude (cm)	Observed	18	17	17	16	15
			Forecasted	5	7	6	6	9
Exp6	AE2	Distance (km)		91	227	277	339	453
		Amplitude (cm)	Observed	16	15	10	7	6
			Forecasted	7	9	6	4	6

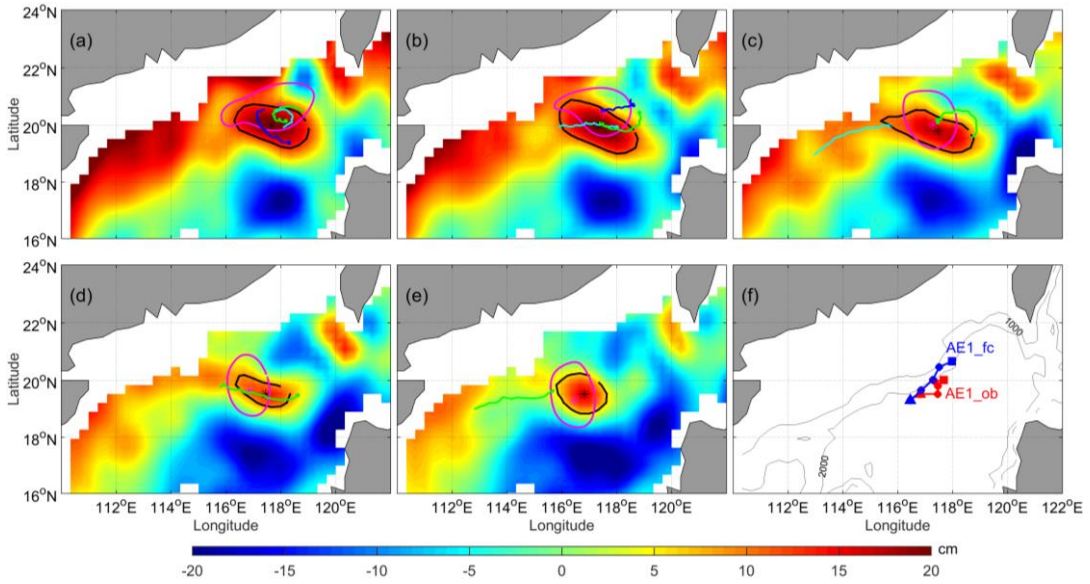

Fig. 8 Comparison of AE1 of Exp1 and observation, and trajectories of drifter buoys during the 29th of November 2003 and the 29th of December 2004. The cyan, green and blue solid circle dots and lines indicated the start positions and trajectories of number 22917, 22918 and 22610 drift buoys during the corresponding period, respectively. Where, the red (blue) dotted line in (f) is the path of AE1 derived from observation (forecast) SLA during the experiment period, the square (triangle) represents the start (end) position.

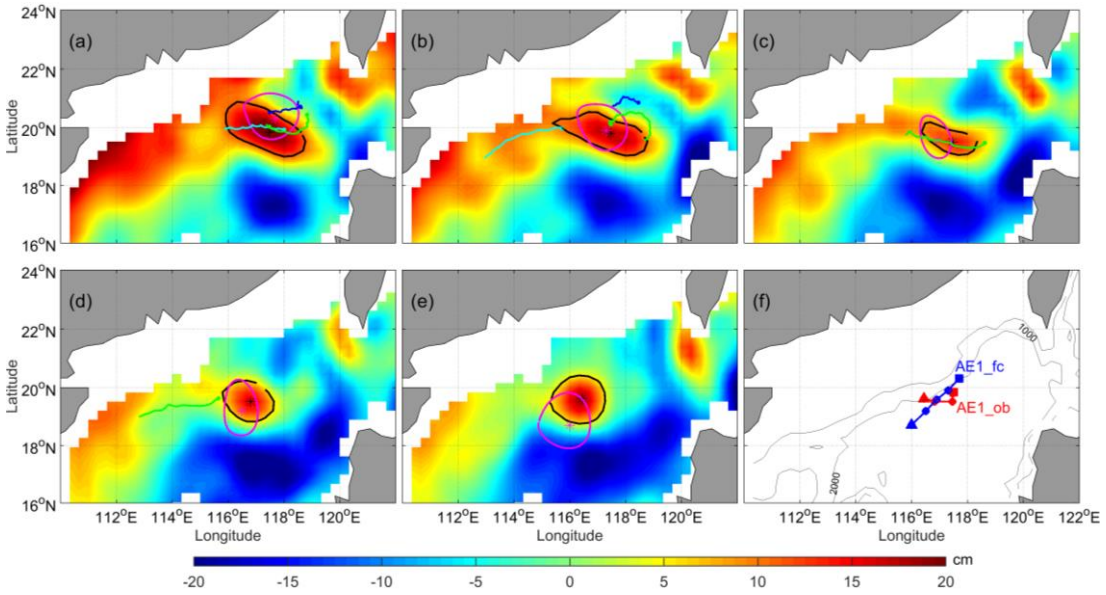

Fig. 9 Same as figure 8, but for Exp2, the experiment period is the 10th of December 2003 to the 9th of January 2004.

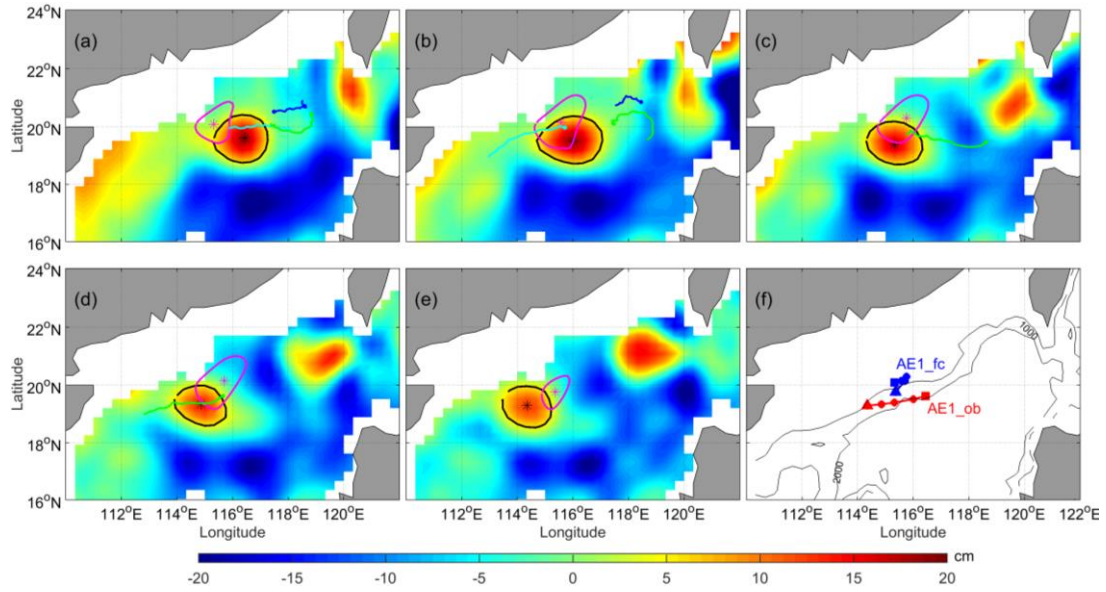

Fig. 10 Same as figure 9, but for Exp3, the experiment period is the 31st of December 2003 to the 30th of January 2004.

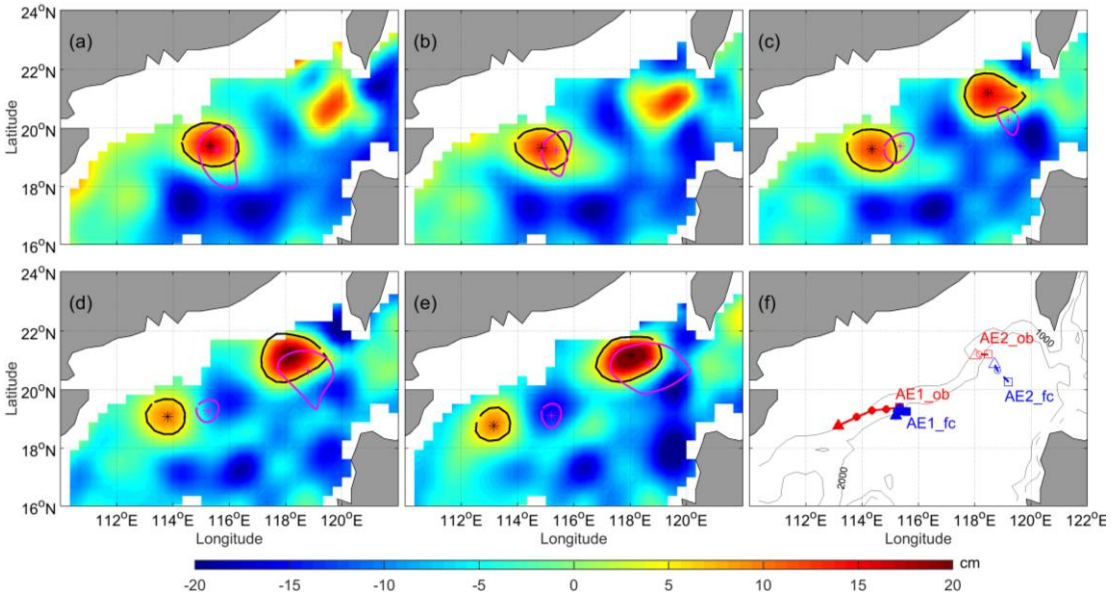

Fig. 11 Same as figure 8, but for Exp4， where, the red (blue) dotted line in (f) is the observation (forecast) moving path of AE1 and AE2. the red solid (dashed) lines and solid (hollow) circle derived from observation SLA for AE1 (AE2), the blue solid (dashed) lines and solid (hollow) circle derived from forecast SLA during the 21st of January 2004 to the 20th of February 2004.

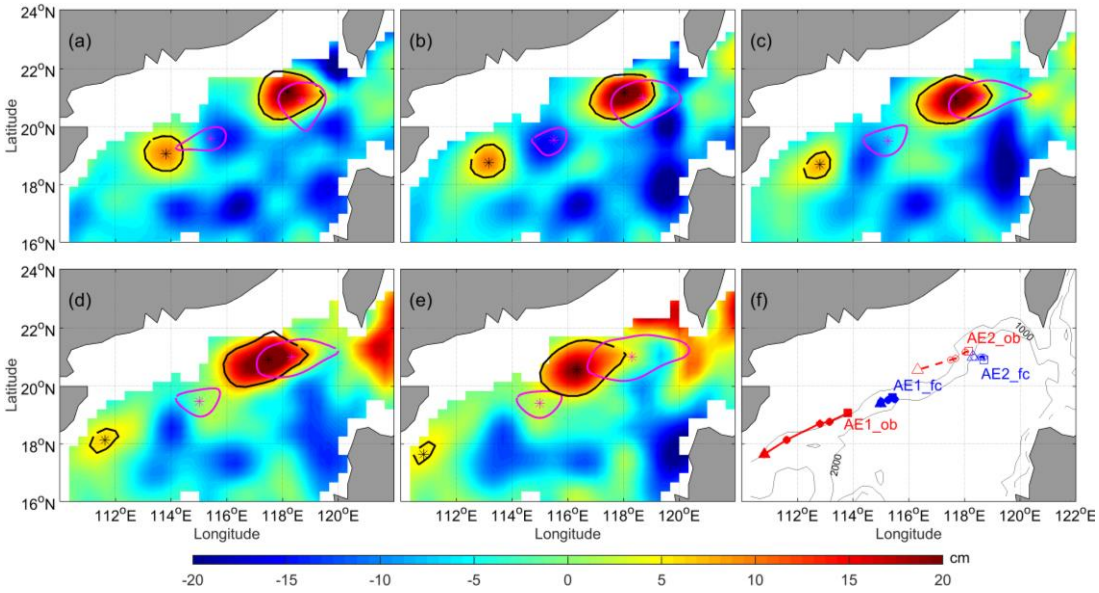

578

579 Fig. 12 Same as figure 11, but for Exp5, the experiment period is the 8th of February 2004 to the 10th of

580 March 2004.

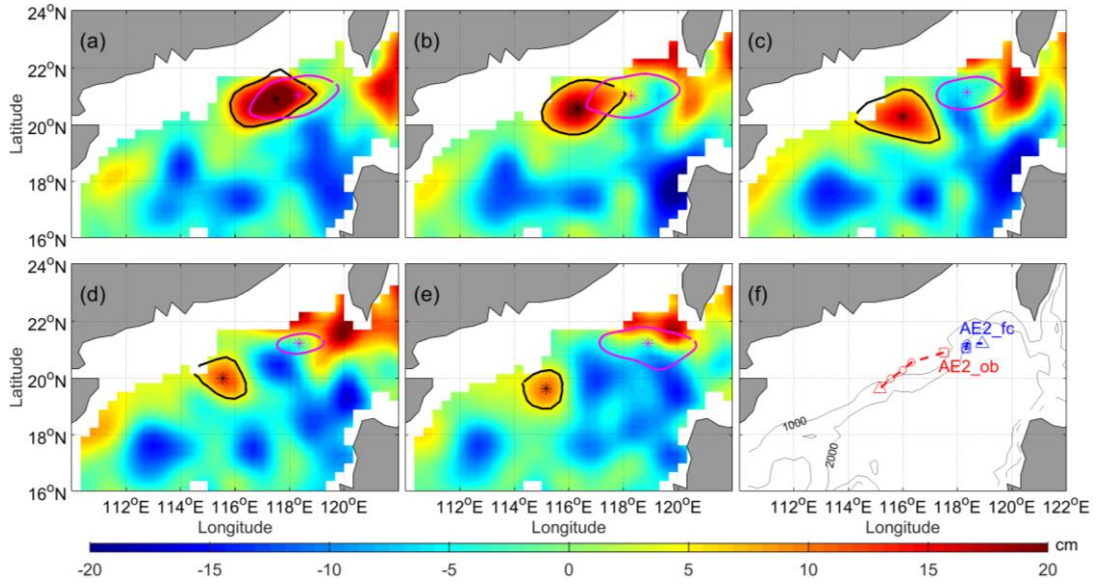

581

582 Fig. 13 Same as figure 11, but for Exp6 and AE2, the experiment period is the 29th of February 2004 to

583 the 30th of March 2004.

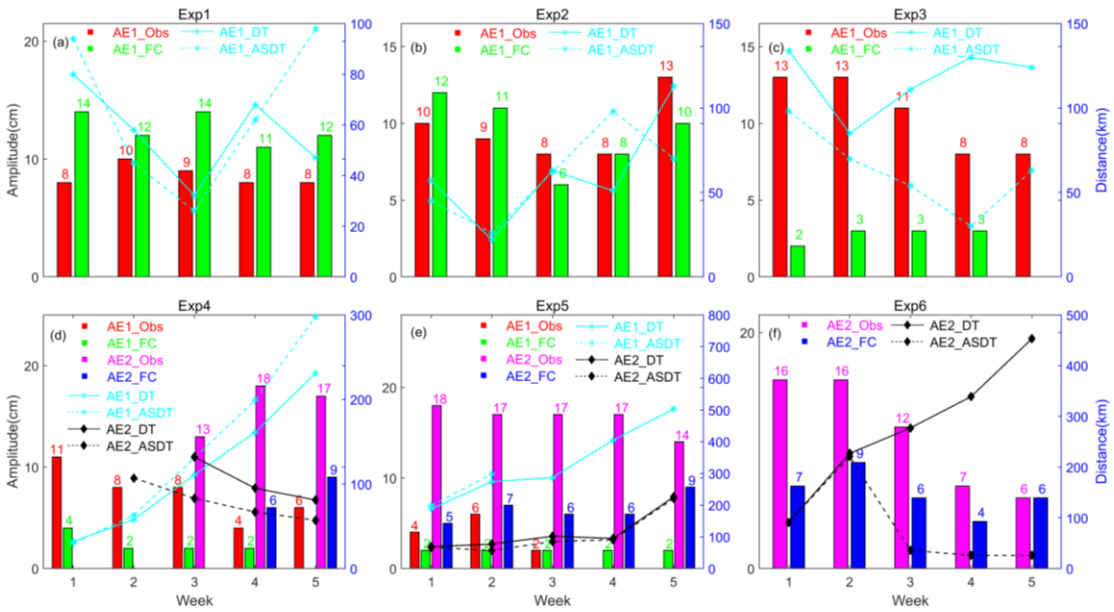

584

585 Fig. 14 The amplitude of AE1 and AE2 derived from observation SLA and the six forecast SLA,
586 and distance of eddy centers between the observation, assimilation and forecast SLA's, respectively.
587 The red and green histograms indicated the AE1 amplitudes from observation and prediction
588 respectively. The pink and blue histograms expressed the AE2 amplitudes from observation and
589 prediction respectively. The cyan star solid (dash) line shows the distance of the center between
590 observation and prediction (assimilation) AE1. The black diamond solid (dash) line shows the
591 distance of the center between observation and prediction (assimilation) AE2.